Vapor-Phase Molecular Doping of Graphene for High-Performance Transparent Electrodes

Youngsoo Kim,[†,‡,#] Jaechul Ryu,[§,⊥,#] Myungjin Park,[†] Eun Sun Kim,[†] Je Min Yoo,[†] Jaesung Park,[∥] Jin Hyoun Kang,[†] and Byung Hee Hong[†,⊥,*]

[†]Department of Chemistry and [‡]Department of Physics & Astronomy, Seoul National University, 1 Gwanak-ro, Seoul 151-742, Korea, [§]Micro Device & Machinery Solution Division, Samsung Techwin R&D Center, Seongnam 463-400, Korea, [⊥]SKKU Advanced Institute of Nanotechnology (SAINT) and Center for Human Interface Nano Technology (HINT), Sungkyunkwan University, Suwon 440-746, Korea, and [∥]Korea Center for Nanometrology, Korea Research Institute of Standards and Science, Gajeong-Ro, Daejon 305-340, Korea. [#]These authors contributed equally.

ABSTRACT Doping is an essential process to engineer the conductivity and work-function of graphene for higher performance optoelectronic devices, which includes substitutional atomic doping by reactive gases, electrical/electrochemical doping by gate bias, and chemical doping by acids or reducing/oxidizing agents. Among these, the chemical doping has been widely used due to its simple process and high doping strength. However, it also has an instability problem in that the molecular dopants tend to gradually evaporate from the surface of graphene, leading to substantial decrease in doping effect with time. In particular, the instability problem is more serious for n-doped graphene because of undesirable reaction between dopants and oxygen or water in air. Here we report a simple method to tune the electrical properties of CVD graphene through n-doping by vaporized molecules at 70 °C, where the dopants in vapor phase are mildly adsorbed on graphene surface without direct contact with solution. To investigate the dependence on functional groups and molecular weights, we selected a series of ethylene amines as a model system, including ethylene diamine (EDA), diethylene triamine (DETA), and triethylene tetramine (TETA) with increasing number of amine groups showing different vapor pressures. We confirmed that the vapor-phase doping provides not only very high carrier concentration but also good long-term stability in air, which is particularly important for practical applications.

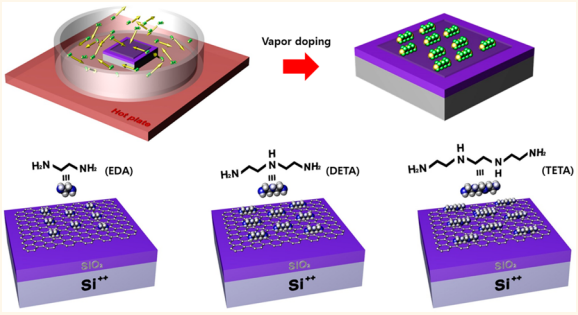

KEYWORDS: graphene · chemical doping · vapor doping · FET · ethylene amine

Graphene has been reported as one of the most fascinating two-dimensional materials[1] owing to its outstanding properties including flexibility,[2] high mobility,[3] transparency,[4] heat dissipation ability,[5] and so further. Recently, graphene has also shown potential to be adopted in optoelectronics[6] or flexible electronics,[7] especially in conducting electrodes due to its unusual band structure[1] and electrical tunability. To employ graphene in practical electronic devices, however, it is necessary to enhance its conductivity and control the work function appropriately, which can be performed by various doping methods including atomic substitution,[8,9] molecular adsorption,[10−13] covalent functionalization,[14−19] substrate induced doping,[20,21] polymerization on graphene,[22,23] and the use of metallic thin films or nanoparticles.[24−26] The substitution of carbon atoms with B or N, as well as the covalent functionalization, is advantageous in terms of long-term stability, which is, however, unfavorable due to significant decrease in carrier mobility and conductivity.

In this regard, the nondestructive and noncovalent doping by chemical species is favored, but it also has an instability problem in that the molecular dopants tend to gradually evaporate from the surface of graphene. This instability issue is more important for n-dopants as it easily reacts with oxygen or water molecules in air. Thus, several groups have suggested stable n-doping methods based on encapsulation by spin-coated polymers[22] and

* Address correspondence to byunghee@snu.ac.kr.

Received for review October 26, 2013 and accepted December 7, 2013.

Published online December 08, 2013
10.1021/nn405596j

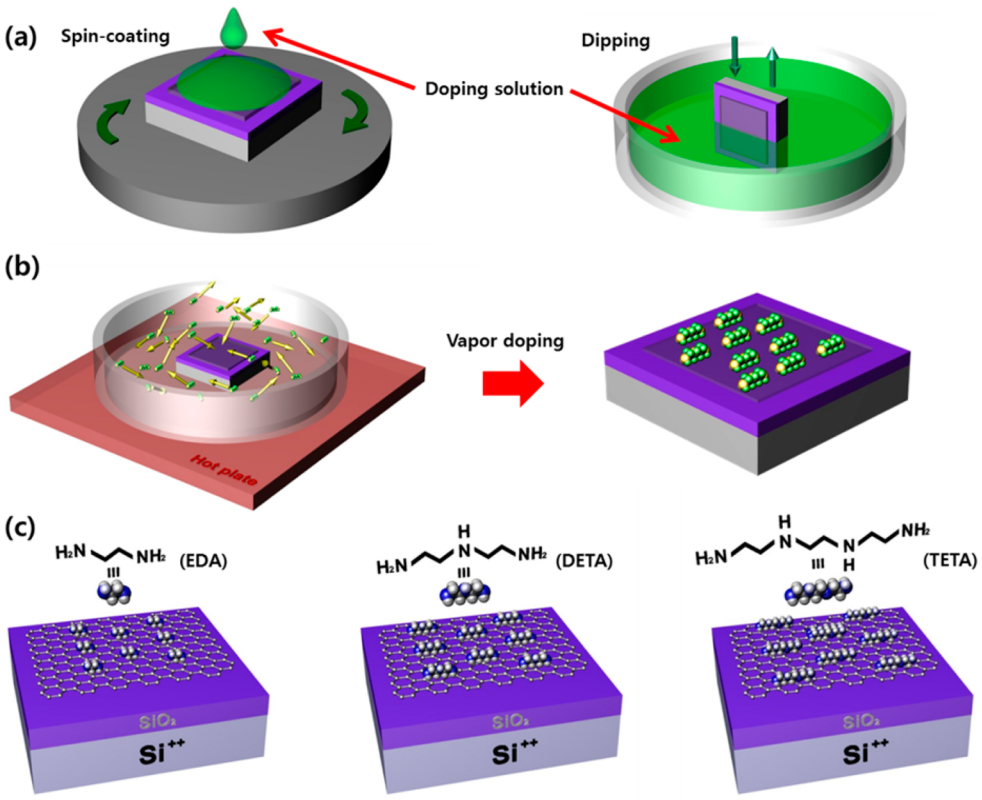

Figure 1. (a) Schematic process of spin-coating process (left) and dipping process (right). (b) Schematic process of evaporation doping. The molecules were evaporated by thermal heating using hot plate (left), then vapor doped graphene was obtained (right). (c) Schematic illustration of ethylene amines doped graphene field effect devices and molecular structure of EDA, DETA, and TETA.

nanoparticles.[27] However, the doping strength of these methods is not strong enough to control the conductivity and work-function of graphene, efficiently. In addition, the doping by spin-coating or dipping (Figure 1a) using highly concentrated and reactive solution often results in contamination or damage by undesirable reactions. For such reasons, developing a highly stable, uniform and nondestructive yet intense n-doping method has been strongly demanded.

Thus, we report a simple method to tune the electrical properties of CVD graphene through n-doping by molecular vapors, where the dopants in vapor phase are mildly adsorbed on graphene surface without direct contact with solution (Figure 1b). To investigate the dependence on functional groups and molecular weights, we selected a series of ethylene amines as a model system, including ethylene diamine (EDA), diethylene triamine (DETA), and triethylene tetramine (TETA) with increasing number of amine groups and different vapor pressures (Table 1 and Figure 1c). The amine group is widely used as a good electron donor for various chemical reactions, which has been utilized as an n-dopant for graphene.[12−14,21] Therefore, it is expected that the amount of electrons injection per covered area increases with the number of amine groups. On the other hand, the vapor pressure of DETA and TETA is very low at ambient condition, so the temperature needs to be elevated for efficient vaporization. Thus, we treated graphene with EDA, DETA, and TETA at 70 °C, and found that the doped graphene exhibits strong and stable n-doping characteristics increasing with number of amine groups. In particular, the sheet resistance of graphene is measured to be 98 ± 12 Ω/sq after doping by TETA, which is believed to the best conductivity for n-doped monolayer graphene. The doping and stability dependence on number of amine groups and molecular weights were carefully studied through atomic force microscopy (AFM), Raman, UV/vis spectroscopy and various electrical measurements at different temperatures as discussed below.

TABLE 1. Comparing of Three Types of Ethylene Amines Molecules

	no. amines	molecular weight (g mol^{-1})	boiling point (°C)	vapor pressure at 20 °C (Pa)	vapor pressure at 70 °C (Pa)[28,29]
EDA	2	60.1	116	1300	∼20000
DETA	3	103.17	204	10	∼460
TETA	4	146.23	267	<1	∼13.5

RESULTS AND DISCUSSION

The characteristics of n-doped graphene were studied by Raman spectroscopy at room temperature

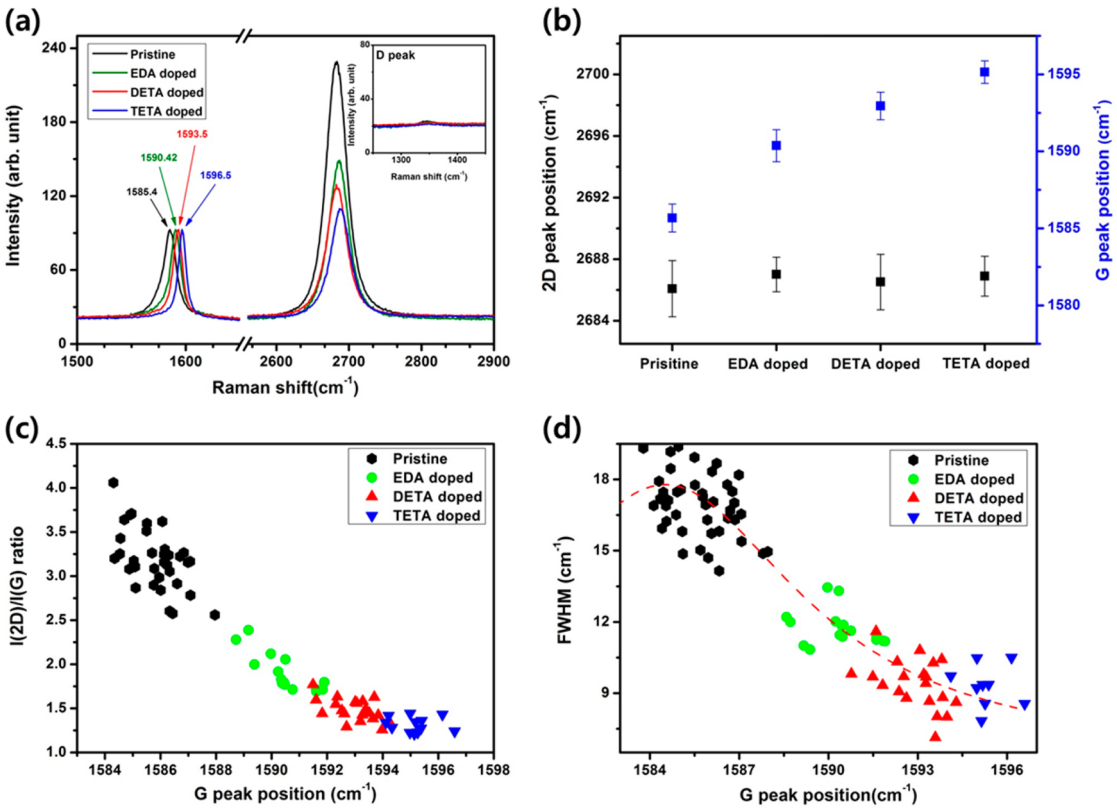

Figure 2. (a) Representative Raman spectra of pristine, EDA, DETA, and TETA doped graphene (inset shows D peaks of representative Raman spectra). (b) G and 2D peak position with pristine and various ethylene amines doped graphene. (c) Intensity ratio of 2D/G as a function of G peak position for each molecule doping. (d) FWHM of G peak as a function of G peak position with pristine and ethylene amines doped graphene (red line is fitted by Lorentzian curve).

with 1 mW 514 nm-laser to minimize possible damage on graphene. Noticeable Raman peaks in graphene are the G band (~1584 cm^{-1}) and the 2D band (~2700 cm^{-1}) involving phonon frequencies near the Γ and K points in the Brillouine Zone.[30] We characterized a pristine graphene and ethylene amine doped graphene samples to compare their Raman features. Figure 2a shows the representative Raman spectra of pristine graphene and doped graphene with EDA, DETA, and TETA.

The G band of graphene was upshifted from 1585.4 cm^{-1} (pristine) to 1590.4 cm^{-1} (EDA), 1593.5 cm^{-1} (DETA) and 1596.5 cm^{-1} (TETA), due to the effect of the Fermi level shift on the phonon frequencies induced by electron doping.[31,32] In addition, the quality of graphene sample can be maintained after vapor doping process as confirmed by the low D peak (Figure 2a, inset) intensity related to defect density. As the number of amine groups in ethylene amine vapors increased (2, 3, and 4 for EDA, DETA, and TETA, respectively), the G peak positions were accordingly upshifted because the graphene became more intensely n-doped. On the contrary, the positions of the 2D peak were consistent regardless of doping (shown in Figure 2b). The different phenomena observed from the G peak and the 2D peak are mentioned in electrochemically gated graphene: The electron density can modify the 2D phonon (adiabatic effect), while the G phonon is affected by electron−phonon coupling (nonadiabatic effect).[33] In other words, the position of the 2D peak is predicted to decrease for an increasing electron concentration, whereas, the blue-shift of the G peak is observed due to electron−phonon coupling. Thus, the blue-shift of the 2D peak is expected for the strongly n-doped graphene, but it was not actually observed in the ethylene amine doped graphene. We suppose that the intermolecular interaction between adsorbed ethylene amine molecules and CVD graphene results in the abnormal shift of 2D peaks.

The intensity ratio of 2D to G peak is another important parameter to estimate the doping intensity.[34] It was shown to decrease when the graphene was doped as shown in Figure 2c. Dozens of random points were measured to yield an average value, and the ratio of *I*(2D)/*I*(G) decreased from 4.0 to 1.2 as a function of the G peak position from 1584 to 1597 cm^{-1}. In Figure 2d, the full width at half-maximum (FWHM) values of the G band for pristine and doped graphene are shown. As the degree of doping intensified, the FWHM decreased due to the forbidden electron−hole pair arose from the Pauli exclusion principle.[33,34] On the basis of these Raman features, we were able to confirm that graphene can

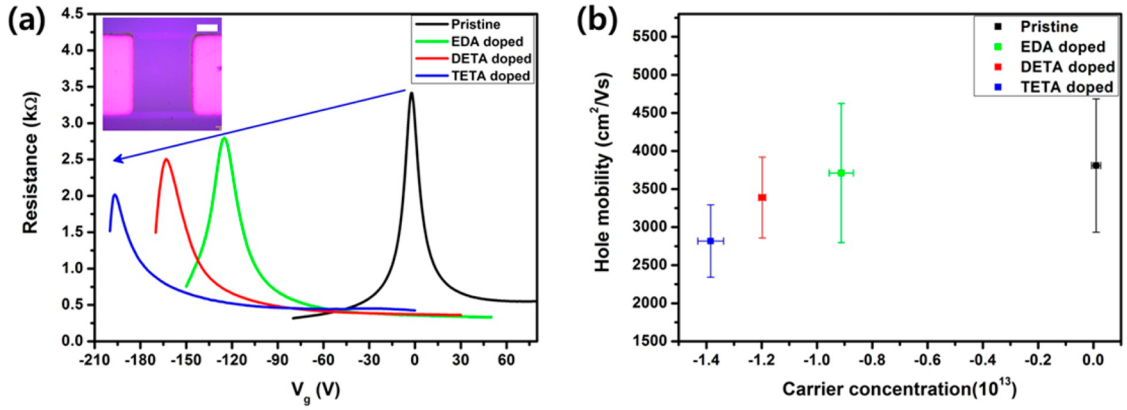

Figure 3. (a) Electrical characteristic of the FET devices of pristine (black), EDA-doped (green), DETA-doped (red), and TETA-doped (blue) graphene. The inset shows an optical image of the graphene FET. Scale bar, 50 μm. (b) Hole mobility of pristine, EDA-, DETA-, and TETA-doped graphene as a function of carrier concentration.

be n-doped by ethylene amine vapors and the data showed a tendency that matches to the number of amine groups in the vapor dopants. In addition, the Raman features of doped graphene samples showed similar trends to the electric field induced tuning of the Dirac point of graphene, upshift of G band peak with decreasing I(2D)/I(G) ratio as a function of doping concentration.[30−34]

To investigate and compare n-doping effects of ethylene amine vapors, the electrical properties of pristine and n-doped graphene transistors were measured. In Figure 3a, representative results of graphene field effect transistors for each molecule (EDA, DETA, and TETA) are displayed with different charge neutral points with respect to the vapors. The Dirac voltage of the pristine graphene transistor was initially measured, which was observed at 1.4 ± 2.3 V. The Dirac voltages were shifted to −126.6 ± 5.8, −166.4 ± 1.8, and −192.3 ± 5.8 V, respectively, for EDA, DETA, and TETA doped graphene (Figure S3).

Graphene field effect devices showed relatively high mobility for their scales (approximately 200 μm scale, optical image provided in the inset of Figure 3a), which can be partially contained grain boundaries, ripples and small cracks in CVD graphene.[35−37] More than 45 pristine graphene devices were measured, yielding 6219 ± 1288 cm^2 V^{-1} s^{-1} (hole region) and 3809 ± 876 cm^2 V^{-1} s^{-1} (electron region) without doping. For the doped graphene devices, we only compared the electron mobility due to the lack of hole-region points. After vapor doping, graphene devices showed decreasing electron mobility of 3711 ± 913, 3388 ± 531, and 2817 ± 475 cm^2 V^{-1} s^{-1}, respectively, for EDA, DETA, and TETA doped transistors. Such trend can be attributed to the potential difference between ethylene amines and pristine graphene; ethylene amines act as impurity charge sources on graphene channel.[23] As shown in Figure 3b, the results were plotted as a function of the carrier concentration, and the carrier concentration can be estimated according to the equation: $n = -\alpha(V_g - V_{CNP})$, with $\alpha = 7.2 \times 10^{11}$ cm^{-2} V^{-1},[1,34] giving approximately 9×10^{12}, 1.2×10^{13}, and 1.4×10^{13} cm^{-2} for respective dopants.

For comparison, the graphene films doped by dipping and spin-coating methods (Figure 1a) were characterized by FET measurements and optical imaging. The result shows that the graphene surface is irregularly covered with dopant molecules (Figure. S3). Therefore, the n-doping effect by dipping and spin-coating is much weaker or inhomogeneous (details in Figure. S4) compared to the vapor-phase doping that shows relatively uniform coverage of dopant molecules on graphene surface as shown in the AFM images (Figure. S5).

Doping stability is another critical issue in fabricating n-doped graphene devices. Ethylene amine doped graphene transistors were studied by measuring the Dirac voltage as a function of the exposure time in the ambient condition for at least two weeks. For this study, CVD graphene films grown from a single batch were used to avoid inconsistencies in graphene devices and doping processes. As shown in Figure 4a−c, the charge neutral points of modified graphene devices doped with EDA, DETA, and TETA abruptly degraded after 36 h of exposure to air. To compare the stability of doping for each vapor, graphene devices with EDA, DETA, and TETA vapors were all measured (shown in Figure 4d). The results of n-doping stability based on the charge neutral points showed similar tendency in three types of devices (EDA, DETA, and TETA doped case) and charge neutral points were observed to start saturating after 36 h of exposure in the ambient condition. After 20 days of exposure in the air, the charge neutral point of graphene field effect transistors were changed from −126.6 ± 5.8 to −56 ± 7.3 V for EDA doped graphene, from −166.4 ± 1.8 to −111.8 ± 3.6 V for DETA doped graphene, and from −192.3 ± 5.8 to −151.4 ± 3.5 V for TETA doped graphene compared to initially doped graphene. The major culprits for such dramatic doping reduction are

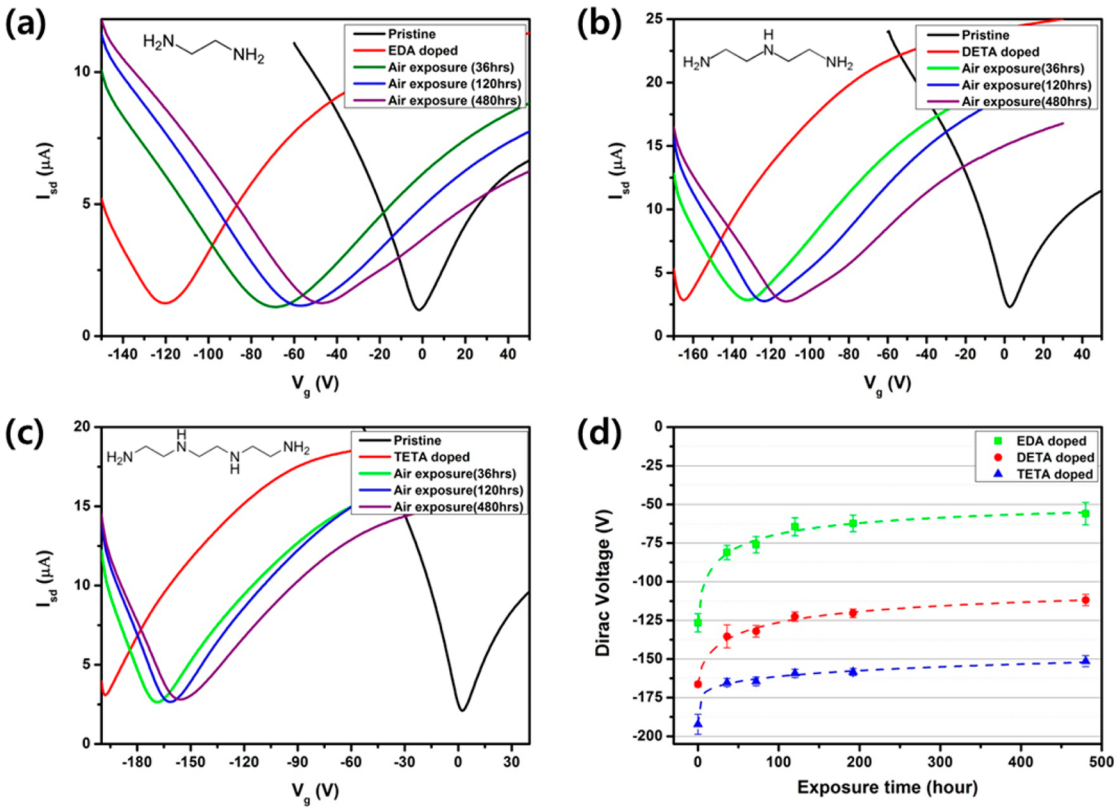

Figure 4. Dirac voltage shift as a function of air exposure time for each molecular doped graphene devices (a) EDA, (b) DETA, and (c) TETA. (d) Statistics of measured n-doped graphene devices.

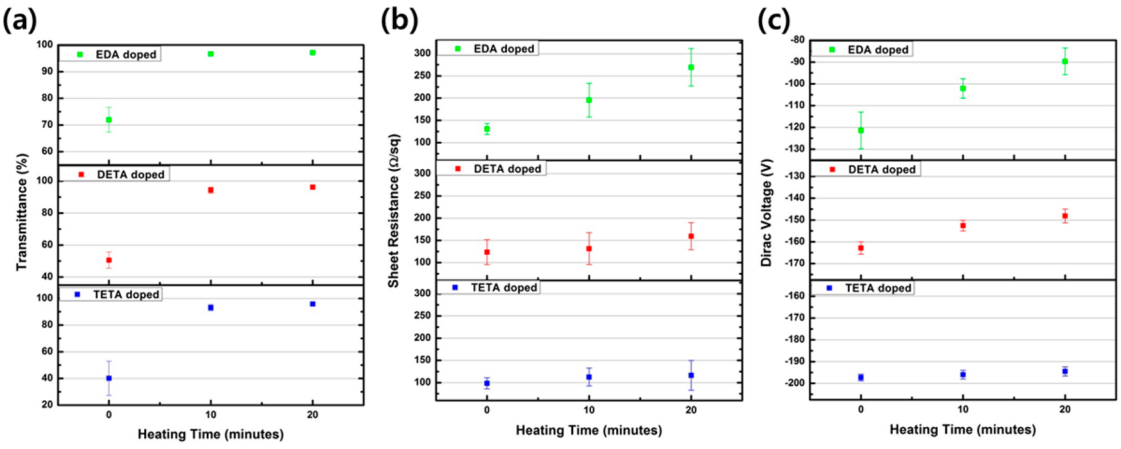

Figure 5. Changes in the transmittance at 550 nm wavelength (a), sheet resistance (b), and Dirac voltage (c) of EDA-, DETA-, and TETA-doped graphene with increasing annealing time at 70 °C.

inevitable evaporation of adsorbed molecules and the absorption of unwanted p-dopant gases on graphene in the ambient air. To check the influence by oxygen or water molecules in air, a pristine graphene FET was measured over 10 days in an ambient condition. We found that the p-doping effect of pristine graphene was saturated after 3 days, and the Dirac voltage was shifted by +30 V compared to as-prepared graphene (Figure S6). In the case of the vapor-doped graphene, the p-doping by ambient air can be minimized as long as the graphene surface is covered with ethylene amine molecule, which would be advantageous for the long-term stability of the strong n-doping effect.

The transmittance of n-doped graphene by ethylene amine vapors is slightly lower than the pristine graphene, because vapor-deposited ethylene amines initially form a lot of light-scattering aggregates on graphene surface. These ethylene amine aggregates can be easily removed by mild thermal heating for longer than 10 min at 70 °C, which eliminates the haze problem and increases the optical transmittance.

In addition, unlike EDA and DETA, TETA still has low vapor pressure at 70 °C (Table 1) and interacts with graphene strongly enough to prevent evaporation, so we can obtain relatively stable sheet resistance and enhanced transmittance for the TETA doped graphene after thermal treatment (Figure 5 and Figure S7). This indicates that the stability of n-doping greatly depends on molecular weight and vapor pressure at given temperature, which needs to be carefully considered in the molecular doping of graphene. It should be also noted that the Dirac voltage change of the n-doped graphene well correlates with the sheet resistance change (Figure 5 and Figure S8), which can be utilized as a simple parameter to optimize the conductivity of graphene.

CONCLUSION

In summary, we demonstrated that graphene can be efficiently n-doped by ethylene amine vapors. The doping strength and stability depends on the number of electron-donating functional groups ($-NH_2$), molecular weight, and vapor pressure of the adsorbed molecules. In particular, the TETA-doped graphene shows very high carrier concentration (1.4×10^{13} cm^{-2}) as well as the lowest monolayer sheet resistance (98 ± 12 Ω/sq) with excellent stability. We expect that the vapor-phase doping of molecular n-dopants will be able to solve the practical problems associated with the limited conductivity, durability, and safety issues of graphene films grown by CVD for further electronic applications.[38−44]

EXPERIMENTAL METHODS

CVD Graphene Synthesis and Device Fabrication. Graphene film was synthesized on a 25 μm thick copper foil through chemical vapor deposition (CVD) method, using methane (50 sccm) and hydrogen (5 sccm) gas with vacuum pumping at 1000 °C. Graphene transfer step was completed according to the conventional processes (Supporting Information S1): PMMA was spin-coated on top of graphene and copper foil was etched in ammoniumpersurfate solution (20 mM with distilled water). Highly p-doped Si substrate covered with a 300 nm thick SiO_2 was used for the electrical measurement of graphene field effect devices. Free-standing graphene on distilled water was carefully transferred to SiO_2/Si substrate and PMMA was removed in acetone. Chrome (5 nm) and gold (30 nm) layers were deposited thermally for metal contact of 3-terminal graphene device with prepatterned stensile mask. Graphene channels were isolated through electron beam lithography. To avoid inconsistent growth condition, we used graphene samples grown from a single batch. Each device was fabricated with 200 μm width and 50−250 μm length. Before doping the graphene film, thermal annealing was carried out at 300 °C for 1 h under argon and hydrogen gas environment to remove PMMA residues and trapped water after device fabrication.

Doping Method. In the vapor-phase doping method, EDA, DETA, and TETA molecules were commercially purchased at Sigma-Aldrich. Vapor doping was carried out in Petri-dish at 70 °C, baking on a hot plate with molecule droplet on tissue for 30 min in air (Figure 1b). Finally, EDA, DETA and TETA molecules were deposited on graphene surface as depicted in Figure 1c. Spin-coating was performed at 3000 rpm speed for 1 min by commercial spin-coater, and graphene on SiO_2 was mildly soaked into doping solution for 30 min. The ethylene amines concentration of 0.1 mol/L in ethanol was used in spin-coating and dipping doping method.

Characterization Method. The Raman spectra were measured using Renishaw inVia Raman Microscope with 1 mW 514 nm Ar laser with the spot size of 2 μm. Topological characterization was measured by using Park System XE-100 atomic force microscope with noncontact mode (to obtain precise morphology, exfoliated graphene was used). UV−vis absorption spectra were recorded on a Varian Cary 5000 spectrophotometer with varying wavelengths from 200 to 800 nm. For UV−vis absorption and sheet resistance measurement, graphene was transferred on PET and SiO_2/Si substrates, and the same doping method was followed. In electrical measurements of graphene field effect transistors, Agilent 2602 was used on 3-terminal geometry with source, drain and gate in air. Constant 10 mV voltage was applied from source to drain during the measurement. The sheet resistance of the graphene (50 μm × 50 μm square geometry) was measured using a four-point probe with a nanovoltmeter (Keithley 6221, 2182A) and the Van der Pauw method was applied. The sheet resistance of graphene was obtained using the following equation:

$$R_s = \frac{\pi}{\ln 2}\frac{V}{I}$$

Conflict of Interest: The authors declare no competing financial interest.

Supporting Information Available: Additional information on the experimental results, including CVD graphene growth and transfer processes and electrical/optical/AFM measurements of pristine and vapor-doped graphene in comparison with spin-coating and dipping methods. This material is available free of charge *via* the Internet at http://pubs.acs.org.

Acknowledgment. This research was supported by the National Research Foundation of Korea funded by the Ministry of Science, ICT & Future (Global Frontier Research Center for Advanced Soft Electronics 2011-0031629, 2011-0017587, 2012M3A7B4049807) and the Research Settlement Fund for the new faculty of SNU.

REFERENCES AND NOTES

1. Novoselov, K. S.; Geim, A. K.; Morozov, S. V.; Jiang, D.; Zhang, Y.; Dubonos, S. V.; Grigorieva, I. V.; Firsov, A. A. Electric Field Effect in Atomically Thin Carbon Films. *Science* **2004**, *306*, 666–669.
2. Lee, Y.; Bae, S.; Jang, H.; Jang, S.; Zhu, S.-E.; Sim, S. H.; Song, Y. I.; Hong, B. H.; Ahn, J.-H. Wafer-Scale Synthesis and Transfer of Graphene Films. *Nano Lett.* **2010**, *10*, 490–493.
3. Bolotin, K. I.; Sikes, K. J.; Jiang, Z.; Klima, M.; Fudenberg, G.; Hone, J.; Kim, P.; Stormer, H. L. Ultrahigh Electron Mobility in Suspended Graphene. *Solid State Commun.* **2008**, *146*, 351–355.
4. Nair, R. R.; Blake, P.; Grigorenko, A. N.; Novoselov, K. S.; Booth, T. J.; Stauber, T.; Peres, N. M. R.; Geim, A. K. Fine Structure Constant Defines Visual Transparency of Graphene. *Science* **2008**, *320*, 1308.
5. Balandin, A. A.; Ghosh, S.; Bao, W.; Calizo, I.; Teweldebrhan, D.; Miao, F.; Lau, C. N. Superior Thermal Conductivity of Single-Layer Graphene. *Nano Lett.* **2008**, *8*, 902–907.
6. Bao, Q.; Loh, K. P. Graphene Photonics, Plasmonics, and Broadband Optoelectronic Devices. *ACS Nano* **2012**, *6*, 3677–3694.
7. Bae, S.; Kim, H.; Lee, Y.; Xu, X.; Park, J.-S.; Zheng, Y.; Balakrishnan, J.; Lei, T.; Kim, H. R.; Song, Y. I.; *et al.* Roll-to-Roll Production of 30-Inch Graphene Films for Transparent Electrodes. *Nat. Nanotechnol.* **2010**, *5*, 574–578.

8. Panchokarla, L. S.; Subrahmanyam, K. S.; Saha, S. K.; Govindaraj, A.; Krishnamurthy, H. R.; Waghmare, U. V.; Rao, C. N. R. Synthesis, Structure, and Properties of Boron- and Nitrogen-Doped Graphene. *Adv. Mater.* **2009**, *21*, 4726–4730.
9. Wei, D. C.; Liu, Y. Q.; Wang, Y.; Zhang, H. L.; Huang, L. P.; Yu, G. Synthesis of N-Doped Graphene by Chemical Vapor Deposition and Its Electrical Properties. *Nano Lett.* **2009**, *9*, 1752–1758.
10. Schedin, F.; Geim, A. K.; Morozov, S. V.; Hill, E. W.; Blake, P.; Katsnelson, M. I.; Novoselov, K. S. Detection of Individual Gas Molecules Adsorbed on Graphene. *Nat. Mater.* **2007**, *6*, 652–655.
11. Ryu, S.; Liu, L.; Berciaud, S.; Yu, Y.-J.; Liu, H.; Kim, P.; Flynn, G. W.; Brus, L. E. Atmospheric Oxygen Binding and Hole Doping in Deformed Graphene on a SiO_2 Substrate. *Nano Lett.* **2010**, *10*, 4944–4951.
12. Dong, X.; Fu, D.; Fang, W.; Shi, Y.; Chen, P.; Li, L.-J. Doping Single-Layer Graphene with Aromatic Molecules. *Small* **2009**, *5*, 1422–1426.
13. Bult, J. B.; Crisp, R.; Perkins, C. L.; Blackburn, J. L. The Role of Dopants in Long-Range Charge Carrier Transport for p-Type and n-Type Graphene Transparent Conducting Thin Films. *ACS Nano* **2013**, *7*, 7251–7261.
14. Lin, Y.-C.; Lin, C.-Y.; Chiu, P.-W. Controllable Graphene N-Doping with Ammonia Plasma. *Appl. Phys. Lett.* **2010**, *96*, 133110.
15. Niyogi, S.; Bekyarova, E.; Itkis, M. E.; Zhang, H.; Shepperd, K.; Hicks, J.; Sprinkle, M.; Berger, C.; Lau, C. N.; deHeer, W. A.; *et al.* Spectroscopy of Covalently Functionalized Graphene. *Nano Lett.* **2010**, *10*, 4061–4066.
16. Englert, J. M.; Dotzer, C.; Yang, G.; Schmid, M.; Papp, C.; Gottfried, J. M.; Steinrück, H.-P.; Spiecker, E.; Hauke, F.; Hirsch, A. Covalent Bulk Functionalization of Graphene. *Nat. Chem.* **2011**, *3*, 279–286.
17. Guo, B.; Liu, Q.; Chen, E.; Zhu, H.; Fang, L.; Gong, J. R. Controllable N-Doping of Graphene. *Nano Lett.* **2010**, *10*, 4975–4980.
18. Usachov, D.; Vilkov, O.; Grüneis, A.; Haberer, D.; Fedorov, A.; Adamchuk, V. K.; Preobrajenski, A. B.; Dudin, P.; Barinov, A.; Oehzelt, M.; *et al.* Nitrogen-Doped Graphene: Efficient Growth, Structure, and Electronic Properties. *Nano Lett.* **2011**, *11*, 5401–5407.
19. Wei, D.; Liu, Y.; Wang, Y.; Zhang, H.; Huang, L.; Yu, G. Synthesis of N-Doped Graphene by Chemical Vapor Deposition and Its Electrical Properties. *Nano Lett.* **2009**, *9*, 1752–1758.
20. Wang, R.; Wang, S.; Zhang, D.; Li, Z.; Fang, Y.; Qiu, X. Control of Carrier Type and Density in Exfoliated Graphene by Interface Engineering. *ACS Nano* **2010**, *5*, 408–412.
21. Park, J.; Lee, W. H.; Huh, S.; Sim, S. H.; Kim, S. B.; Cho, K.; Hong, B. H.; Kim, K. S. Work-Function Engineering of Graphene Electrodes by Self-Assembled Monolayers for High-Performance Organic Field-Effect Transistors. *J. Phys. Chem. Lett.* **2011**, *2*, 841–845.
22. Wei, P.; Liu, N.; Lee, H. R.; Adijanto, E.; Ci, L.; Naab, B. D.; Zhong, J. Q.; Park, J.; Chen, W.; Cui, Y.; *et al.* Tuning the Dirac Point in CVD-Grown Graphene through Solution Processed n-Type Doping with 2-(2-Methoxyphenyl)-1,3-dimethyl-2,3-dihydro-1H-benzoimidazole. *Nano Lett.* **2013**, *13*, 1890–1897.
23. Deshpande, A.; Sham, C.-H.; Alaboson, J. M. P.; Mullin, J. M.; Schatz, G. C.; Hersam, M. C. Self-Assembly and Photopolymerization of Sub-2 nm One-Dimensional Organic Nanostructures on Graphene. *J. Am. Chem. Soc.* **2012**, *134*, 16759–16764.
24. Pi, K.; McCreary, K. M.; Bao, W.; Han, W.; Chiang, Y. F.; Li, Y.; Tsai, S. W.; Lau, C. N.; Kawakami, R. K. Electronic Doping and Scattering by Transition Metals on Graphene. *Phys. Rev. B* **2009**, *80*, 075406.
25. Chen, J. H.; Jang, C.; Adam, S.; Fuhrer, M. S.; Williams, E. D.; Ishigami, M. Charged-Impurity Scattering in Graphene. *Nat. Phys.* **2008**, *4*, 377–381.
26. Huh, S.; Park, J.; Kim, K. S.; Hong, B. H.; Kim, S. B. Selective n-Type Doping of Graphene by Photo-patterned Gold Nanoparticles. *ACS Nano* **2011**, *5*, 3639–3644.
27. Ho, P.-H.; Yeh, Y.-C.; Wang, D.-Y.; Li, S.-S.; Chen, H.-A.; Chung, Y.-H.; Lin, C.-C.; Wang, W.-H.; Chen, C.-W. Self-Encapsulated Doping of n-Type Graphene Transistors with Extended Air Stability. *ACS Nano* **2012**, *6*, 6215–6221.
28. Ethyleneamines—A Global Profile of Products and Services, Huntsman Corporation, 2007.
29. Efimova, A. A.; Emel'yanenko, V. N.; Verevkin, S. P.; Chernyak, Y. Vapour Pressure and Enthalpy of Vaporization of Aliphatic Poly-Amines. *J. Chem. Thermodyn.* **2010**, *42*, 330–336.
30. Ferrari, A. C.; Meyer, J. C.; Scardaci, V.; Casiraghi, C.; Lazzeri, M.; Mauri, F.; Piscanec, S.; Jiang, D.; Novoselov, K. S.; Roth, S.; *et al.* Raman Spectrum of Graphene and Graphene Layers. *Phys. Rev. Lett.* **2006**, *97*, 187401.
31. Pisana, S.; Lazzeri, M.; Casiraghi, C.; Novoselov, K. S.; Geim, A. K.; Ferrari, A. C.; Mauri, F. Breakdown of the adiabatic Born−Oppenheimer Approximation in Graphene. *Nat. Mater.* **2007**, *6*, 198–201.
32. Lee, J. E.; Ahn, G.; Shim, J.; Lee, Y. S.; Ryu, S. Optical Separation of Mechanical Strain from Charge Doping in Graphene. *Nat. Commun.* **2012**, *3*, 1024.
33. Das, A.; Pisana, S.; Chakraborty, B.; Piscanec, S.; Saha, S. K.; Waghmare, U. V.; Novoselov, K. S.; Krishnamurthy, H. R.; Geim, A. K.; Ferrari, A. C.; *et al.* Monitoring Dopants by Raman Scattering in an Electrochemically Top-Gated Graphene Transistor. *Nat. Nanotechnol.* **2008**, *3*, 210–215.
34. Casiraghi, C.; Pisana, S.; Novoselov, K. S.; Geim, A. K.; Ferrari, A. C. Raman Fingerprint of Charged Impurities in Graphene. *Appl. Phys. Lett.* **2007**, *91*, 233108.
35. Yu, Q.; Jauregui, L. A.; Wu, W.; Colby, R.; Tian, J.; Su, Z.; Cao, H.; Liu, Z.; Pandey, D.; Wei, D.; *et al.* Control and Characterization of Individual Grains and Grain Boundaries in Graphene Grown by Chemical Vapour Deposition. *Nat. Mater.* **2011**, *10*, 443–449.
36. Huang, P. Y.; Ruiz-Vargas, C. S.; van der Zande, A. M.; Whitney, W. S.; Levendorf, M. P.; Kevek, J. W.; Garg, S.; Alden, J. S.; Hustedt, C. J.; Zhu, Y.; *et al.* Grains and Grain Boundaries in Single-Layer Graphene Atomic Patchwork Quilts. *Nature* **2011**, *469*, 389–392.
37. Ni, G. X.; Zheng, Y.; Bae, S.; Kim, H. R.; Pachoud, A.; Kim, Y. S.; Tan, C. L.; Im, D.; Ahn, J. H.; Hong, B. H.; Ozyilmaz, B. Quasi-Periodic Nanoripples in Graphene Grown by Chemical Vapor Deposition and Its Impact on Charge Transport. *ACS Nano* **2012**, *6*, 1158–1164.
38. Kim, K. S.; Zhao, Y.; Jang, H.; Lee, S. Y.; Kim, J. M.; Kim, K. S.; Ahn, J.-H.; Kim, P.; Choi, J.-Y.; Hong, B. H. Large-Scale Pattern Growth of Graphene Films for Stretchable Transparent Electrodes. *Nature* **2009**, *457*, 706–710.
39. Kang, J.; Kim, H.; Kim, K. S.; Lee, S. K.; Bae, S.; Ahn, J.-H.; Kim, Y. J.; Choi, J. B.; Hong, B. H. High-Performance Graphene-Based Transparent Flexible Heaters. *Nano Lett.* **2011**, *11*, 5154–5158.
40. Ha, J.; Park, S.; Kim, D.; Ryu, J.; Lee, C.; Hong, B. H.; Hong, Y. High-Performance Polymer Light Emitting Diodes with Interface-Engineered Graphene Anodes. *Org. Electron.* **2013**, *14*, 2324–2330.
41. Han, T.-H.; Lee, Y.; Choi, M.-R.; Woo, S.-H.; Bae, S.-H.; Hong, B. H.; Ahn, J.-H.; Lee, T.-W. Extremely Efficient Flexible Organic Light-Emitting Diodes with Modified Graphene Anode. *Nat. Photonics* **2012**, *6*, 105–110.
42. Kang, J.; Shin, D.; Bae, S.; Hong, B. H. Graphene Transfer: Key for Applications. *Nanoscale* **2012**, *4*, 5527–5537.
43. Bae, S.; Kim, S. J.; Shin, D.; Ahn, J. H.; Hong, B. H. Towards Industrial Applications of Graphene Electrodes. *Phys. Scr.* **2012**, *T146*, 014024.
44. Jo, S. B.; Park, J.; Lee, W. H.; Cho, K.; Hong, B. H. Large-Area Graphene Synthesis and Its Application to Interface-Engineered Field Effect Transistors. *Solid State Commun.* **2012**, *152*, 1350–1358.